



# Optics Letters

## Optical coherence tomography split-spectrum amplitude-decorrelation optoretinography

SIYU CHEN,<sup>1,2,\*</sup> SHUIBIN NI,<sup>1,2</sup> ALFONSO JIMÉNEZ-VILLAR,<sup>1,2</sup> YIFAN JIAN,<sup>1,2</sup> YALI JIA,<sup>1,2</sup> AND DAVID HUANG<sup>1,2</sup>

<sup>1</sup>Casey Eye Institute, Oregon Health and Science University, Portland, Oregon 97239, USA

<sup>2</sup>Department of Biomedical Engineering, Oregon Health and Science University, Portland, Oregon 97239, USA

\*chensiy@ohsu.edu

Received 31 March 2023; revised 27 June 2023; accepted 29 June 2023; posted 30 June 2023; published 20 July 2023

This pilot study reports the development of optical coherence tomography (OCT) split-spectrum amplitude-decorrelation optoretinography (SSADOR) that measures spatially resolved photoreceptor response to light stimuli. Using spectrally multiplexed narrowband OCT, SSADOR improves sensitivity to microscopic changes without the need for cellular resolution or optical phase detection. Therefore, a large field of view (up to  $3 \times 1 \text{ mm}^2$  demonstrated) using conventional OCT instrument design can be achieved, paving the way for clinical translation. SSADOR promises a fast, objective, and quantifiable functional biomarker for photoreceptor damage in the macula. © 2023 Optica Publishing Group

<https://doi.org/10.1364/OL.492178>

Photoreceptors are specialized sensory neurons and the site of phototransduction. To monitor disease progression, and to evaluate clinical trial safety and efficacy often require direct assessment of visual function. Recently, adaptive optics (AO) optical coherence tomography (OCT) using phase-sensitive detection recorded nanometer scale shrinkage and elongation of photoreceptor outer segments following flash stimuli—revealing the first steps of visual perception [1–4]. The technology, named optoretinogram (ORG), as the optical analogy to electroretinogram (ERG), promises a noninvasive, fast, objective, and quantifiable functional photoreceptor biomarker. Indeed, ORG has revealed increasingly diminished cone response along the transition zone in retinitis pigmentosa (RP) eyes [5].

Despite its successful demonstration, challenges still remain for wider clinical adoption [6,7]. AO instruments are complex and expensive. Imaging field of view is constrained by the iso-planatic patch, often requiring extensive montaging to locate and capture most pathologies. Efforts have been made to measure the ORG phase without AO [8–10]. Yet, detection is vulnerable to noise, necessitating fast imaging technologies that are not ready for commercialization or are limited in sampling locations.

An alternative approach is to detect light-induced alterations in OCT band brightness or boundary position [6,11]. However, intensity-based ORG has not achieved the same consistency or capability as their phase-based counterpart. To address these limitations, we explored the hypothesis that OCT

amplitude decorrelation can provide spatially resolved ORG without resolving single cells and can cover a large retinal area.

This pilot, observational study recruited and imaged adult participants without known or history of retinal disease at the Casey Eye Institute, Oregon Health & Science University (OHSU). The study protocol was approved by the institutional review board (IRB) at OHSU. Written informed consent was obtained from each participant before imaging. The subjects were dark adapted for 5 minutes, but did not undergo mydriasis or cycloplegia.

Using a prototype ultrahigh resolution spectral domain OCT (UHR SD-OCT) instrument and split-spectrum amplitude-decorrelation algorithm, we successfully detected and measured photoreceptor response in 12 normal eyes from 12 adults following test flash (mean years of age  $\pm$  standard deviation,  $41.2 \pm 6.5$ ; range, 33–50). The UHR SD-OCT prototype instrument has previously been reported by the authors [12]. Briefly, the OCT spectrum has a bandwidth of 147 nm centered at 850 nm, corresponding to a full width at half maximum (FWHM) axial resolution of  $2.4 \mu\text{m}$  in air ( $\sim 1.8 \mu\text{m}$  in the retina). The incident beam diameter is  $1.8 \text{ mm}$  ( $1/e^2$ ), with a theoretical FWHM transverse resolution of  $\sim 10 \mu\text{m}$  on the retina. The A-scan rate is 250 kHz.

OCT imaging uses partially coherent light, where scattering or length changes can introduce OCT amplitude variations (speckle). Such fluctuations can be detected using decorrelation-based algorithms, which were previously adopted by OCT angiography (OCTA) [13]. Tuning the OCT coherence length by altering the effective bandwidth can amplify decorrelation. For example, split-spectrum amplitude-decorrelation angiography (SSADA) achieved  $>2$  times improvement on decorrelation signal-to-noise ratio (SNR) in retinal OCTA [14]. A recent OCT functional imaging study also reported that spectrum splitting increased intrinsic optical signal contrast from frog retina [15]. Splitting the spectrum increases the effective OCT coherence length. Therefore, the more pronounced amplitude fluctuation is consistent with an early study using an AO scanning laser ophthalmoscope (SLO), where the authors observed photoreceptor “scintillating” post flash when coherent imaging light was used [16]. Inspired by these studies, we developed split-spectrum amplitude-decorrelation optoretinography (SSADOR).

SSADOR uses volume-repeat scans to obtain a spatially resolved photoreceptor response. Optimizing the parameters

governing the imaging field of view, sampling density, and repeat interval, the rectangular raster scan protocol consists of  $600 \times 200$  A-scans covering a  $10^\circ \times 3.3^\circ$  scan angle (corresponding to a nominal  $3\text{ mm} \times 1\text{ mm}$  retinal area). Consequently, each volume takes 0.5 s. The SSADOR dataset consists of five continually scanned volumes without pause, lasting a total of 2.5 s.

A co-aligned projector delivers the SSADOR test flash. The flash combines 450-nm, 523-nm, and 642-nm light, creating a “white” stimulus. The test flash has a vertical strip pattern extending  $9^\circ$  horizontally (2.8 mm nominal), with alternating bright (4 strips) and dark (3 strips) areas. The vertical extent of the stimulus overlaps the OCT scanning area. This flash pattern has a large background area (~44%), which provides a reference background to evaluate OCT spatial registration performance and investigate noise characteristics. Future clinical studies can use a test flash pattern with very little or no dark areas.

The flash has a retina irradiance of  $1.5\text{ mW/cm}^2$  (illuminance  $\sim 0.3\text{ lm/cm}^2$ ), lasting 200 ms and bleaching 15% of cone pigments [17]. The onset of the flash coincides with the beginning of the third OCT volume, resulting in 2 pre-flash and 2 post-flash volumes. The third OCT volume partially overlaps with the light stimuli. A stationary dim cross in the center of the field provides fixation to maintain forward gaze, which bleaches  $\ll 1\%$  of the cone pigment.

SSADOR calculation is between two OCT volumes, which indicates a two-step approach: (1) spatial registration for correcting eye movements; and (2) quantifying OCT amplitude fluctuations that originate from photoreceptor response.

The spatial registration algorithm adapted a previously published method that used a non-rigid parallel strip geometry [18]. The algorithm was also extended to three dimensions to compensate for movement in the axial (depth) direction. First, the OCT amplitude of the second input (i.e., the moving volume) was scaled to match the dynamic range of the first input (i.e., the reference). We then initialized the transverse displacement field using the whole projected *en face* structure image and cross correlation based rigid translation.

A multilevel pyramid optimization approach refines the initial estimation. Specifically, the moving OCT projection is successively divided along the slow scan direction into overlapping strips of  $500\text{ }\mu\text{m}$ ,  $125\text{ }\mu\text{m}$ , and  $75\text{ }\mu\text{m}$ , respectively. The strips were offset by  $5\text{ }\mu\text{m}$  (i.e., one B-scan). A gradient search updates the affine transformation assigned to each strip to minimize the sum of squared errors. For each A-scan, we calculate the corresponding mean transverse displacement from all parallel strips containing it. Axial displacement is subsequently calculated using nearest A-scan pairs and cross correlation.

With the refined 3D displacement field, we first shift each A-scan axially using the Fourier translation property. Then, transverse correction is performed using Makima piecewise cubic Hermite interpolation, repeated at all depths. Figure 1 shows a representative algorithm output and registration performance. UHR SD-OCT can reliably visualize single scatters within the extent of the photoreceptor outer segment. We believe the scatters are associated with the photoreceptors and have sizes below the imaging resolution, therefore providing an estimation of the point spread function (PSF). The exemplar PSF from the registered and merged volume pairs had a broadening  $< 3\text{ }\mu\text{m}$  as compared to the unmerged reference volume [Figs. 1(d) and 1(e)]. Using the same approach, we estimated the mean FWHM resolution from all nine foveal centered scans (nine eyes from

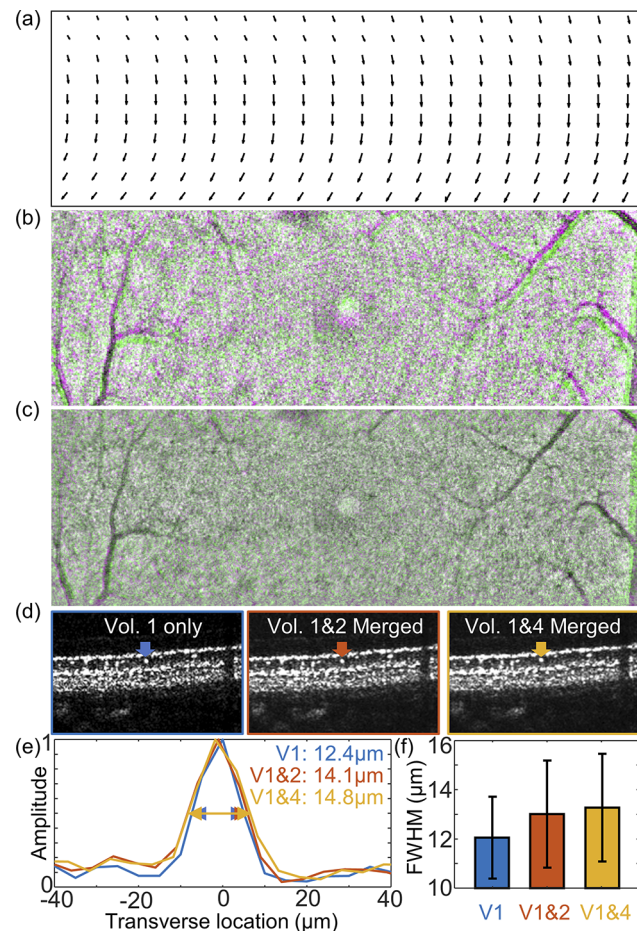


**Fig. 1.** Estimating and correcting for eye movements. (a) Exemplar transverse displacement field for registering the moving OCT volume to the reference. (b) Overlaid, pseudo colored OCT projections from the unregistered reference and moving volumes. (c) Overlaid, pseudo colored OCT projections after spatial registration. Aligned pixels display as gray, misaligned pixels show up as either magenta or green. (d) Enlarged OCT B-scans of the outer retina at the same location from 1 unmerged reference and 2 pairs of registered and merged volumes: reference volume 1; volume 1 and 2 (i.e., before the test flash); and volume 1 and 4 (i.e., after the test flash). Arrows point to the same small isolated scatter within the extent of photoreceptor outer segment. (e) Transverse OCT amplitude profile of the scatter from the reference and two merged and registered volumes. (f) Mean  $\pm$  standard deviation of estimated PSF FWHM using single (V1) and registered, merged volumes (pairs V1 + 2 and V1 + 4). Calculated using nine foveal centered SSADOR scans from nine eyes of nine subjects.

nine subjects). Merged volumes showed minimal PSF widening, which again suggested a registration accuracy well below the OCT resolution [Fig. 1(f)].

Calculating the split-spectrum amplitude-decorrelation follows spatial OCT registration. We empirically chose a 4-fold split using a Gaussian window function and short-time Fourier transform (STFT) to generate four pairs of wavelength multiplexed OCT volumes. The selected 4 $\times$  spectral split corresponds to an increased coherence length of  $\sim 20\text{ }\mu\text{m}$  ( $\sim 10\text{-}\mu\text{m}$  axial resolution). This coherence length is approximately one third to one half of the length of the photoreceptor outer segments [19].

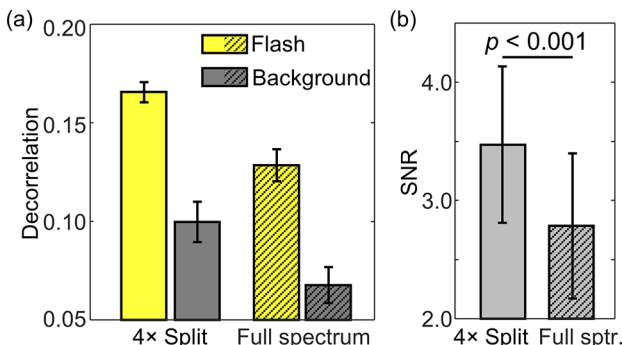


**Fig. 2.** Splitting the OCT spectrum increases mean amplitude decorrelation and improves decorrelation SNR. (a) Mean decorrelation from the flashed and background area. Splitting the spectrum leads to higher decorrelation values in both areas. (b) Decorrelation SNR is significantly higher when calculated using 4× split spectrum as compared to using the full spectrum (nine eyes from nine subjects, two sample *t*-test).

Using all STFT narrowband OCT pairs, we calculated the amplitude decorrelation ( $D$ ) using the following formula:

$$D(x, y, z) = \frac{1}{M} \sum \frac{[A_{1,\lambda}(x, y, z) - A_{2,\lambda}(x, y, z)]^2}{A_{1,\lambda}^2(x, y, z) + A_{2,\lambda}^2(x, y, z)},$$

where  $A_{n,\lambda}(x, y, z)$  denotes the OCT amplitude;  $(x, y, z)$  are the spatial coordinates;  $n, \lambda$  differentiate the two input OCT volumes and the spectral bands, respectively; and  $M$  is the number of splits (SSADOR  $M = 4$  in this study;  $M = 1$  is a special case for full spectrum amplitude decorrelation).

The voxel wise decorrelation is integrated over a 10-μm depth range that encompasses the photoreceptor outer segment tip and posterior portion of the outer segment. We did not differentiate between cones and rods. However, it is expected that cones contribute most to our measurements because of the imaging eccentricity and flash protocol. SSADOR calculation can use either of the two pre-flash volumes as the reference. We did not find statistically significant differences between them, except when obvious motion artifacts exist. Therefore, we selected the volume with less motion as the reference. If the two volumes were similar, the second one was used, acknowledging the fact that it would be temporally closer to the later volumes. This study used the fourth and fifth OCT volume (starting 0.5 s and 1.0 s after test flash onset, respectively) for calculating SSADOR. We found that the choice of either volumes did not affect the calculated mean decorrelation ( $D$ ) or decorrelation SNR. Decorrelation SNR is defined as the decorrelation difference between flashed and background regions, normalized by background standard deviation. This observed temporal stability is consistent with published ORG studies on photoreceptor response dynamics [1,2,4], and is further discussed later. Therefore, unless otherwise noted, the SSADOR map generated from the volume with less motion was used for subsequent analysis.

Mean decorrelation using the 4× spectral split SSADOR algorithm was higher than that of the full spectrum approach ( $0.166 \pm 0.005$  versus  $0.128 \pm 0.008$ ; Fig. 2), averaged from nine scans centered on the fovea of nine eyes. Improvement on decorrelation SNR was modest but statistically significant ( $3.5 \pm 0.6$  versus  $2.8 \pm 0.6$ ,  $p < 0.001$ ). The lower than expected SNR improvement is partially because the split narrowband OCT has less spectral sample points and therefore higher noise

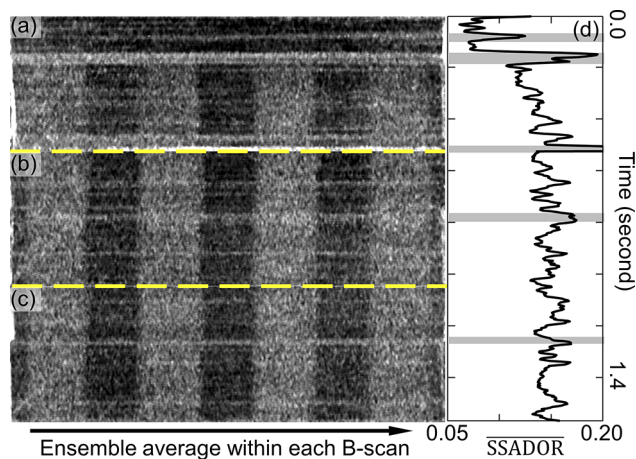


**Fig. 3.** SSADOR provides an ensemble estimation of photoreceptor temporal response. (a)–(c) SSADOR map spatially encoding the temporal signature of photoreceptor response, assuming they share the same dynamics within the imaging field. The maps correspond to the (a) third, (b) fourth, and (c) fifth volumes in the dataset. (d) Averaging SSADOR decorrelation ( $\overline{\text{SSADOR}}$ ) within each B-scan and converting B-scan indices to time generate a time trace of photoreceptor response. Maximum response is reached between 0.3 and 0.5 s, and remains a plateau for the entire scan duration (1.5 s). Shaded area, excessive eye movements.

[20]. SSADOR may also be more sensitive to motion and flow projection artifacts compared with full spectrum decorrelation. Investigations are ongoing to suppress these noises and further SNR improvement.

Despite the limited volume repeat rate (2 Hz), SSADOR can characterize the temporal photoreceptor response, assuming they share similar dynamics within the imaging field. Using all three post flash volumes (i.e., volume 3, 4, and 5) and averaging the SSADOR signal within each B-scan, Fig. 3 plots the ensemble response against time. It revealed a rapid rise within 0.5 s following the flash onset. Maximum SSADOR decorrelation reached a plateau from approximately 0.5 s to 1.5 s (end of the dataset). This temporal dynamic is consistent with reported measurements from single photoreceptors using AO and phase-based approaches [1,2,4].

Finally, we investigated if SSADOR can detect and quantify changes in photoreceptor adaptation. In addition to the SSADOR test flash, we introduced an intense flash to bleach photoreceptor pigments. The single bleaching flash had an irradiance of  $4.1 \text{ mW/cm}^2$  (illuminance  $\sim 1.0 \text{ lm/cm}^2$ ), covering the inferior half of the imaged field and lasting 200 ms. It bleached approximately 36% of exposed cone pigments [17]. SSADOR scans were obtained before and after the bleaching flash. The imaging field was 1.5 mm inferior to the fovea. The vertical scan size was reduced to 150 A-scans ( $2.5^\circ$  or  $0.75 \text{ mm}$  nominal), which led to a slightly shorter volume interval of 0.38 s. This reduction was to account for the reduced fixation stability following the intense bleaching flash.

We performed the measurement on three eyes from three healthy adults (Fig. 4). SSADOR decorrelation was 14% lower ( $0.160 \pm 0.005$  versus  $0.138 \pm 0.003$ ), and decorrelation SNR was 49% lower ( $3.37 \pm 0.21$  versus  $1.71 \pm 0.05$ ) 5 s after the bleaching flash. Both SSADOR decorrelation and decorrelation SNR recovered to  $>94\%$  at 1 min ( $0.153 \pm 0.005$  and  $3.17 \pm 0.12$ , respectively). Using one-way analysis of variance (ANOVA)

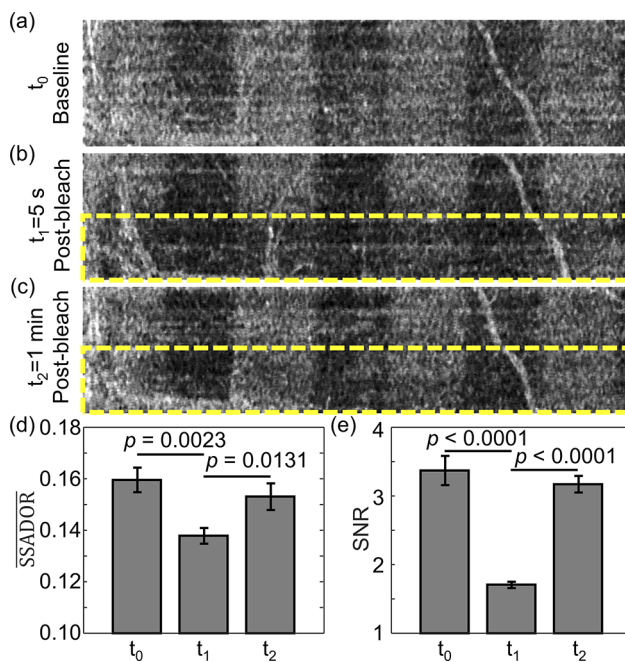


**Fig. 4.** Exemplar SSADOR photoreceptor response map before and after an intense bleach. Three measurement time points, corresponding to (a) the baseline  $t_0$ , (b) 5-second post bleach  $t_1$ , and (c) 1-minute post bleach  $t_2$ , are shown. The yellow dashed box indicates the bleached area. (d) Mean SSADOR decorrelation (SSADOR) and (e) decorrelation SNR within the bleached area from three healthy adults.

followed by post hoc paired *t*-test corrected for multiple comparisons ( $m = 3$ ), the responsivity reduction at the 5-s time point is statistically significant.

This pilot study proved that the combination of UHR SD-OCT and SSADOR can detect and measure functional photoreceptor response to light stimuli, without the need for complex AO or phase-sensitive detection. Collectively, the advancements enable functional photoreceptor imaging using OCT instrument and raster scan protocols that are compatible with current commercial implementations, removing a significant barrier for clinical translation. One highlight is the relatively large field of view (3 mm  $\times$  1 mm) and short measurement time (2.5 s). Using automated imaging montage, the macula (approximately 6 mm  $\times$  6 mm) can be covered with 6 scans (15-s total imaging time). Future technological advancements (e.g., spectrometer speed) will proportionally improve the measurement field of view and reduce testing times. Preliminary data indicate SSADOR decorrelation is positively correlated with test flash strength. A follow up study will quantitatively investigate this dose dependency.

Limitations of the study also warrant discussion. This study used a fixed 4 $\times$  spectral split. However, an eccentricity-based strategy that accounts for topographical variations in photoreceptor outer segment length may be necessary for imaging fields outside the macula [19]. The SSADOR decorrelation is not directly correlated to physical changes (e.g., reflectiv-

ity and length), which require additional investigations. Future algorithmic improvement on OCT spatial registration and flow projection artifact removal can increase the SNR and improve measurement sensitivity.

In conclusion, UHR SD-OCT and SSADOR promise to provide a clinically translatable functional biomarker for characterizing photoreceptor damage.

**Funding.** National Eye Institute (P30 EY010572); Research to Prevent Blindness; Edward N. and Della L. Thome Memorial Foundation; BrightFocus Foundation.

**Disclosures.** Yifan Jian, Seymour Vision Inc. (I); Yali Jia, Visionix Inc. (F, P); David Huang, Visionix Inc. (F, P,); Other authors declare no conflicts of interest.

**Data availability.** Data underlying the results presented in this paper are not publicly available at this time but may be obtained from the authors upon reasonable request.

## REFERENCES

- D. Hillmann, H. Spahr, C. Pfäffle, H. Sudkamp, G. Franke, and G. Hüttmann, *Proc. Natl. Acad. Sci. U. S. A.* **113**, 13138 (2016).
- M. Azimipour, J. V. Migacz, R. J. Zawadzki, J. S. Werner, and R. S. Jonnal, *Optica* **6**, 300 (2019).
- F. Zhang, K. Kurokawa, A. Lassoued, J. A. Crowell, and D. T. Miller, *Proc. Natl. Acad. Sci. U. S. A.* **116**, 7951 (2019).
- V. P. Pandiyan, A. Maloney-Bertelli, J. A. Kuchenbecker, K. C. Boyle, T. Ling, Z. C. Chen, B. H. Park, A. Roorda, D. Palanker, and R. Sabesan, *Sci. Adv.* **6**, eabc1124 (2020).
- A. Lassoued, F. Zhang, K. Kurokawa, Y. Liu, M. T. Bernucci, J. A. Crowell, and D. T. Miller, *Proc. Natl. Acad. Sci. U. S. A.* **118**, e2107444118 (2021).
- R. S. Jonnal, *Ann. Transl. Med.* **9**, 1270 (2021).
- N. Wynne, J. Carroll, and J. L. Duncan, *Prog. Retinal Eye Res.* **83**, 100920 (2021).
- S. Tomczewski, P. Węgrzyn, D. Borycki, E. Auksorius, M. Wojtkowski, and A. Curatolo, *Biomed. Opt. Express* **13**, 2186 (2022).
- K. V. Vienola, D. Valente, R. J. Zawadzki, and R. S. Jonnal, *Optica* **9**, 1100 (2022).
- X. Jiang, T. Liu, V. P. Pandiyan, E. Slezak, and R. Sabesan, *Biomed. Opt. Express* **13**, 5989 (2022).
- T.-H. Kim, G. Ma, T. Son, and X. Yao, *Front. Med.* **9**, 864824 (2022).
- B. Lee, S. Chen, E. M. Moul, Y. Yu, A. Y. Alibhai, N. Mehta, C. R. Baumal, N. K. Waheed, and J. G. Fujimoto, *Transl. Vis. Sci. Technol* **9**, 12 (2020).
- R. F. Spaide, J. G. Fujimoto, N. K. Waheed, S. R. Sadda, and G. Staurenghi, *Prog. Retinal Eye Res.* **64**, 1 (2018).
- Y. Jia, O. Tan, J. Tokayer, B. Potsaid, Y. Wang, J. J. Liu, M. F. Kraus, H. Subhash, J. G. Fujimoto, and J. Horngger, *Opt. Express* **20**, 4710 (2012).
- D. Thapa, B. Wang, Y. Lu, T. Son, and X. Yao, *J. Mod. Opt.* **64**, 1800 (2017).
- R. S. Jonnal, J. Rha, Y. Zhang, B. Cense, W. Gao, and D. T. Miller, *Opt. Express* **15**, 16141 (2007).
- A. Paupoo, O. Mahroo, C. Friedburg, and T. Lamb, *J. Physiol.* **529**, 469 (2000).
- P. Zang, G. Liu, M. Zhang, C. Dongye, J. Wang, A. D. Pechauer, T. S. Hwang, D. J. Wilson, D. Huang, D. Li, and Y. Jia, *Biomed. Opt. Express* **7**, 2823 (2016).
- C. A. Curcio, J. D. Messinger, K. R. Sloan, A. Mitra, G. McGwin, and R. F. Spaide, *Invest. Ophthalmol. Visual Sci.* **52**, 3943 (2011).
- M. A. Choma, M. V. Sarunic, C. Yang, and J. A. Izatt, *Opt. Express* **11**, 2183 (2003).